

Numerical optimization of microfluidic biosensor detection time for the SARS-CoV-2 using the Taguchi method

I Ben Mariem¹, S Kaziz^{2,3*} , M Belkhiria¹, F Echouchene^{1,4} and H Belmabrouk^{1,5}

¹Electronic and Microelectronics Lab, Department of Physics, Faculty of Science of Monastir, University of Monastir, 5019 Monastir, Tunisia

²Quantum and Statistical Physics Laboratory, Faculty of Sciences of Monastir, University of Monastir, Environment Boulevard, 5019 Monastir, Tunisia

³Higher National Engineering School of Tunis, Taha Hussein Montfleury Boulevard, University of Tunis, 1008 Tunis, Tunisia

⁴Higher Institute of Applied Sciences and Technology of Sousse, University of Sousse, Sousse, Tunisia

⁵Department of Physics, College of Science at Zulfi, Majmaah University, Al Majma'ah 11952, Saudi Arabia

Received: 23 October 2022 / Accepted: 06 February 2023 / Published online: 11 March 2023

Abstract: The performance of microfluidic biosensor of the SARS-Cov-2 was numerically analyzed through finite element method. The calculation results have been validated with comparison with experimental data reported in the literature. The novelty of this study is the use of the Taguchi method in the optimization analysis, and an $L8(2^5)$ orthogonal table of five critical parameters—Reynolds number (Re), Damköhler number (Da), relative adsorption capacity (σ), equilibrium dissociation constant (K_D), and Schmidt number (Sc), with two levels was designed. ANOVA methods are used to obtain the significance of key parameters. The optimal combination of the key parameters is $Re = 10^{-2}$, $Da = 1000$, $\sigma = 0.2$, $K_D = 5$, and $Sc = 10^4$ to achieve the minimum response time (0.15). Among the selected key parameters, the relative adsorption capacity (σ) has the highest contribution (42.17%) to the reduction of the response time, while the Schmidt number (Sc) has the lowest contribution (5.19%). The presented simulation results are useful in designing microfluidic biosensors in order to reduce their response time.

Keywords: ANOVA; Biosensor; Detection time; SARS-CoV-2; Taguchi method

1. Introduction

Coronavirus disease 2019 (COVID-19) is a new infectious disease caused by the severe acute respiratory syndrome coronavirus-2 (SARS-CoV-2). This new virus appeared in China at the end of December 2019, quickly spread throughout the planet and caused many deaths [1, 2]. Therefore, quick measures were taken to limit the transmission of a disease we do not yet fully understand. Among these measures, scientists around the world have sought to improve the detection of SARS-CoV-2 devices [3].

Recently, there has been a growing interest in integrating advanced biosensors into laboratory systems on a chip by introducing microfluidics [4]. Microfluidic biosensors have played an essential role in the fight against this

pandemic [5–7]. Among the detection methods, we can cite surface plasmon resonance (SPR) sensor [8, 9], quartz crystal microbalance (QCM) sensor [10, 11], and immunoassays [12, 13]. These methods involve the same specific binding kinetics of analytes and immobilized ligands. The binding efficiency on the reaction surface is generally great enough to bind virtually all the analyte molecules that appear there. In this case, the reaction is said to be transport limited and it generally causes the formation of a diffusion boundary layer which reduces the performance of microfluidic biosensors [14]. To enhance the analyte transport, several experimental and numerical approaches have been developed [15–25]. Analytes and ligands immobilized binding reaction on the sensitive surface lead to the formation of analyte–ligand complexes on this surface, the concentration of which has a determining role for the detection process [19, 26]. SARS-CoV-2 uses its structural S-spike glycoprotein (S protein) to bind

*Corresponding author, E-mail: kaziz_sameh@yahoo.fr

to the angiotensin-converting enzyme (ACE2) located at the surface of the human cell [27].

Currently, most laboratories use a molecular method called “quantitative real-time polymerase chain reaction” (qRT-PCR) for the virus’s detection in respiratory infections. This method is well established, it can detect even tiny amounts of viruses [5, 28], but it requires well-equipped laboratories, it can also take time and above all it can be prone to errors [29].

Many studies have shown that several manufacturing parameters can be adjusted to enhance the performance of biosensors [15, 17–23, 30–33]. Shahbazi et al. [31] studied the impact of certain conception parameters on the saturation time of biosensors intended for the recognition of coronaviruses. Their study revealed that moving the reaction surface position by just 500 μm decreased the saturation time by further than 50%.

In this study, we performed 2D finite element simulation on the kinetics of SARS-CoV-2 binding reaction to optimize the microfluidic biosensor performances. To determine the degree of influence of some input factors on the biosensor detection time, Taguchi’s numerical plan of experiment, based on analysis of variance (ANOVA) and mean effects, was adopted as a support for the modeling of the microfluidic biosensor, in order to have the minimum simulation to be performed. The Taguchi method is a powerful tool for identifying the optimal combination of design parameters to reduce cost, improve quality and/or increase efficiency. Therefore, the optimal level of the process parameters corresponds to the one with the highest signal-to-noise (S/N) ratio [34]. Optimizing the biosensor through the design of experiments helps guide efforts to improve the performance of future sensing devices.

The Taguchi approach is used in many domains such as physics [35], medicine [36], environmental sciences [37, 38], chemical processes [39] and statistics [40]. ANOVA is one of the most common methods used for analyzing the data. It is a statistical technique that assesses potential differences in a scale-level dependent variable by a nominal-level variable having two or more categories.

2. Physical model

2.1. Microfluidic biosensor design

As illustrated in Fig. 1, the microfluidic biosensor studied has a length (L) of 250 μm and a height (H) of 40 μm , and the reaction surface, of 20 μm and 3 μm dimensions, respectively, is located on the bottom wall of the microchannel. The carrier fluid, which is water, mixed with the analytes (SARS-CoV-2) circulates in the microchannel

from left to right. Ligands (antibodies) are initially immobilized on the reaction surface.

2.2. Pressure and velocity modeling

The fluid, supposed to be Newtonian and incompressible, flows in a laminar and isothermal regime. The Navier–Stokes equations are thus used to determine the pressure and the flow velocity field of the fluid in the microchannel. These equations were considered as dimensionless quantities [41] (Eqs. 1, 2):

$$\nabla^* \cdot \vec{u}^* = 0 \quad (1)$$

$$\left(\vec{u}^* \cdot \nabla^*\right) \vec{u}^* = -\nabla^* p^* + \frac{1}{Re} \Delta^* \vec{u}^* \quad (2)$$

where $Re = \frac{\rho u_0 H}{\mu}$ represents the Reynolds number, ρ and μ are, respectively, the water’s density and the dynamic viscosity, u_0 is the average fluid velocity at the microchannel inlet, and H is the microchannel height. $p^* = \frac{p}{p_0} = \frac{p}{\rho u_0^2}$ is the dimensionless pressure, and $u^* = \frac{u}{u_0}$ is the dimensionless velocity.

2.3. Analyte concentration modeling

The transport of aimed analytes by diffusion and convection is modeled by the following equation (Eq. 3):

$$\frac{\partial C^*}{\partial t^*} + P_e \vec{u}^* \cdot \nabla^* C^* = \Delta^* C^* \quad (3)$$

where $C^* = \frac{C}{C_0}$ is the dimensionless concentration of the analyte, and $t^* = \frac{t}{t_0}$ is the dimensionless time. C and C_0 are the bulk and the inlet analyte concentration, $P_e = \frac{u_0 H}{D}$ is the Peclet number, and D is the diffusion constant of the analyte. The time scale is $t_0 = \frac{H^2}{D}$.

2.4. Complex concentration modeling

The first-order Langmuir–Hinshelwood adsorption model [42, 43] (Eq. 4) was used to calculate the complex concentration of analyte–ligand formed on the surface reaction.

$$\frac{\partial B^*}{\partial t^*} = D_a \sigma \left[C_{\text{surf}}^* (1 - B^*) - K_D B^* \right] \quad (4)$$

where $B^* = \frac{B}{B_{\text{max}}}$, B is the bound complex concentration, and B_{max} is the immobilized ligand concentration on the reaction surface. $C_{\text{surf}}^* = \frac{C_{\text{surf}}}{C_0}$ is the dimensionless analyte concentration near the reaction surface, C_{surf} is the analyte concentration near the reaction surface, $D_a = \frac{K_{\text{on}} B_{\text{max}} H}{D}$ is the Damköhler number, $\sigma = \frac{H C_0}{B_{\text{max}}}$ is the relative density of analyte–ligand complex, and $K_D = \frac{k_{\text{off}}}{k_{\text{on}} C_0}$ is the

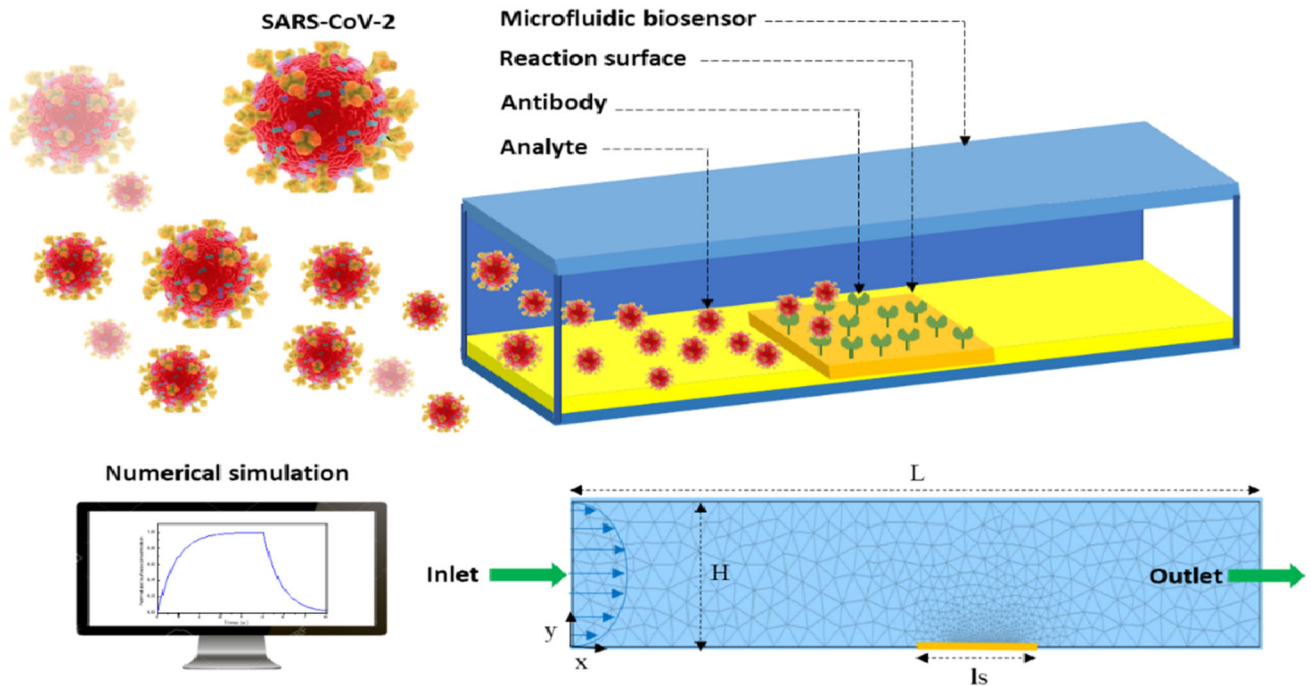


Fig. 1 Microfluidic biosensor design

dimensionless equilibrium constant. k_{on} and k_{off} are the association and dissociation rate constants.

2.5. Boundary and initial conditions

All the boundary conditions for velocity and analyte concentration used in this model are summarized in Table 1 where \vec{n}^* is the unit normal vector to the surface. For the fluid flow, the non-slip conditions are applied to the side surfaces of the microfluidic device, a parabolic velocity profile with average value u_0 is given to the carrier fluid at the inlet, and at the outlet the flow is assumed fully developed. For analyte transport and binding reaction, a low concentration of analyte C_0 is injected at the inlet and the convective flow condition is applied at the outlet. On the sensitive surface, the diffusive flux condition generated by the binding reaction between analytes and ligands is applied and the homogeneous Neumann condition is used

for the other walls and the electrodes because they are assumed to be impermeable and do not interact with the target analyte [31].

The initial velocity of the fluid within the microchannel was assumed to be zero. The concentration of analyte $C_{(t^*=0)}^*$, and the surface analyte/ligand concentration, $B_{(t^*=0)}^*$ was initially zero. The fluid physical parameters and SARS-CoV-2 /Antibody binding parameters [44] used for the simulation are shown in Table 2.

2.6. Numerical method

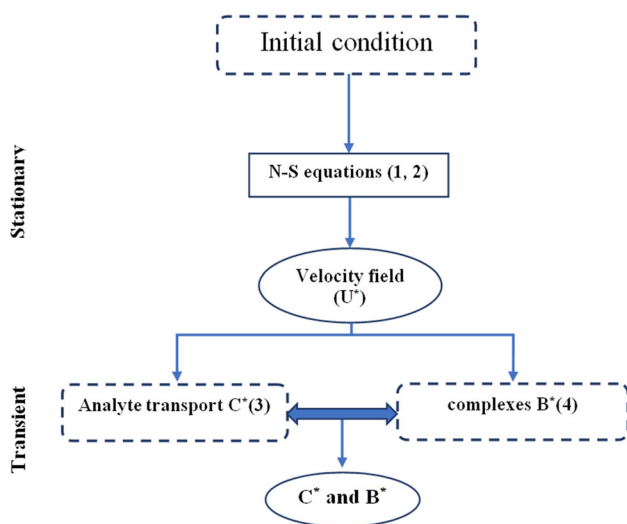
The proposed model equations were solved by finite element method [45]. First, the pressure and velocity fields were calculated by simultaneously solving stationary Eqs. (1) and (2). The concentration of analytes and the concentration of the bound analyte–ligand complexes, formed on the binding surface, were simulated

Table 1 Boundaries conditions used in this simulation

Type	Velocity	Concentration
Walls	$u^* = 0$	$-\vec{n}^* \cdot (-\nabla^* C^* + C^* u^* Pe) = 0$
Sensor	$u^* = 0$	$-\vec{n}^* \cdot (-\nabla^* C^* + C^* u^* Pe) = Da [C_{\text{surf}}^* (1 - B^*) - K_D B^*]$
Inlet	$u_0^* = 1$	$C_0^* = 1$
Outlet	$(\nabla^* u^* + (\nabla^* u^*)^t) \cdot \vec{n}^* = 0$	$\vec{n} \cdot (-\vec{\nabla}^* C^*) = 0$

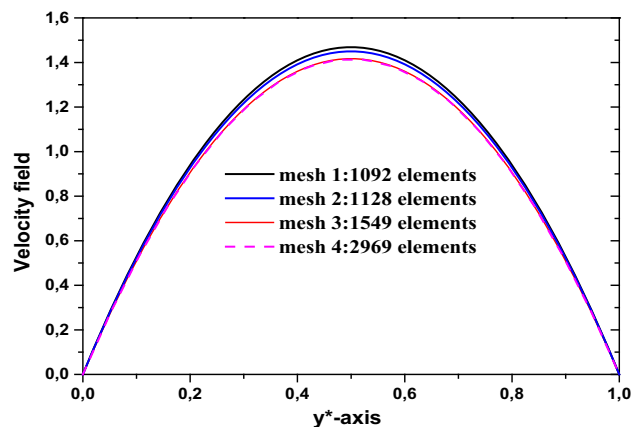
Table 2 Physical and binding parameters [44]

Parameter	Description	Value	Unit
ρ	Fluid density	10^3	kg/m ³
μ	Dynamic viscosity	1.08×10^{-3}	Pa s
k_{on}	Adsorption constant	10^3	m ³ /mol s
k_{off}	Desorption constant	10^{-3}	s ⁻¹
D	Diffusion constant	10^{-10}	m ² /s
B_{max}	Ligand concentration	10^{-8}	mol/m ²
C_0	Analyte input concentration	10^{-5}	mol/m ³

**Fig. 2** Flow chart of numerical simulation

from the coupled time-dependent Eqs. (3) and (4). In the numerical model, the reaction surface is considered as a boundary condition where the diffusion flux is balanced against the reaction rate. The complex concentration at the binding surface is obtained by integrating its spatial value over the reaction surface length. Figure 2 presents a block diagram of the algorithm used to solve this problem.

In order to ensure convergence and that the calculated results are independent of the mesh size, several mesh sizes were tested. Figure 3 presents the velocity field along the y^* -axis for different mesh sizes. When one passes from mesh 1 (1092 elements) to mesh 3 (1549 elements), the calculated solution varies notably. However, additional mesh size refinements slightly affect the numerical solution. We used 1549 triangular geometric elements for the whole 2D domain, including the refined elements of the reaction surface which clearly proves that the convergence is indeed achieved.

**Fig. 3** Velocity profile along the y -axis for several mesh**Table 3** Optimization parameters and their levels

Symbol	Optimization parameter	Level 1	Level 2
Re	Reynolds number	5×10^{-3}	10^{-2}
Da	Damköhler number	5	10^3
σ	Relative adsorption capacity	0.02	0.2
K_D	Equilibrium dissociation constant	1	5
Sc	Schmidt number	5×10^3	10^4

For the analyte transport equation and the chemical kinetics equation, the convergence criterion is chosen such that:

$$\left| \frac{S_{n+1} - S_n}{S_n} \right| \leq \text{Tol}$$

where S_n is the solution at iteration n , and S_{n+1} is the solution at iteration $n + 1$. Tol is the tolerance chosen for the evaluation of a stopping criterion which is 10^{-6} .

2.7. Experimental design

The experiment using Taguchi method was considered in this numerical simulation in order to reduce the response time of microfluidic biosensor. Table 3 shows five factors and two levels used in the experiment design. If two levels were assigned to each of these factors and a factorial experimental design was employed using each of these values, number of permutations would be 32. In order to reduce this number, the orthogonal array of L8, based on Taguchi method, was used and is represented in Table 4. This design requires eight experiments with five simulation parameters at two levels of each neglecting the interactions between them.

Table 4 Taguchi’s L8(25) orthogonal array

Standard order	Factors				
	Re	Da	σ	K_D	Sc
1	1	1	1	1	1
2	1	1	1	2	2
3	1	2	2	1	1
4	1	2	2	2	2
5	2	1	2	1	2
6	2	1	2	2	1
7	2	2	1	1	2
8	2	2	1	2	1

In Taguchi design of experiment (DOE), while designing the experiments, it is necessary to define the input parameters and their levels in order to choose the appropriate orthogonal array (OA) which can significantly reduce the number of experiments. The number of factor is user defined and depends on process knowledge. The low and high levels for each factor we tested are deduced from our own previous work on microfluidic biosensors for the detection of SARS-CoV-2 [17–19, 22, 35] and from the work of other authors [31]. In other words, we have chosen reasonable intervals of these studied parameters.

3. Results and discussion

3.1. Model validation

First, the numerical model was tested by comparison with experimental existing data of Berthier and Silberzan [42],

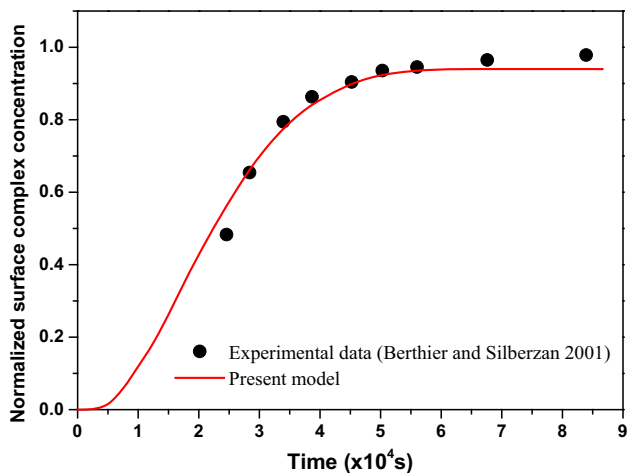


Fig. 4 Validation of the present model with the experimental data of Berthier and Silberzan [42]

as shown in Fig. 4. The time-normalized surface concentration during the adsorption phase was calculated using the same experimental parameters [44], for a microfluidic of 10 mm in length and 1 mm in height.

We can note that the average error between the two results is very small (less than 5%) which makes it possible to consider that the model is validated, and that it can be used for other applications.

Following the successful model validation, eight numerical simulations were performed using the combinations of design parameters in the specified orthogonal matrix table. Figure 5 illustrates the average normalized complex concentration in the reaction surface for all experiment number of Table 4. The curves are plotted as the average surface concentration of complexes $\langle B^* \rangle$ versus dimensionless time.

$$\langle B^* \rangle = \frac{1}{l_s^*} \int_0^{l_s^*} B(x) dx \tag{5}$$

where $l_s^* = \frac{l_c}{H}$ is the dimensionless length of the reaction surface.

The response time of the microfluidic biosensor constitutes the main parameter of the analyte–ligand chemical kinetics. It corresponds to the time during which the concentration of the complex reaches its threshold value. Table 5 shows the numerical results for the response time of microfluidic biosensor using the experimental layout (Table 4).

In order to estimate the effect of the design parameters and to set the relative importance of each design parameter, an analysis of means and variance was carried out following the matrix experiments and the obtaining of all the numerical data.

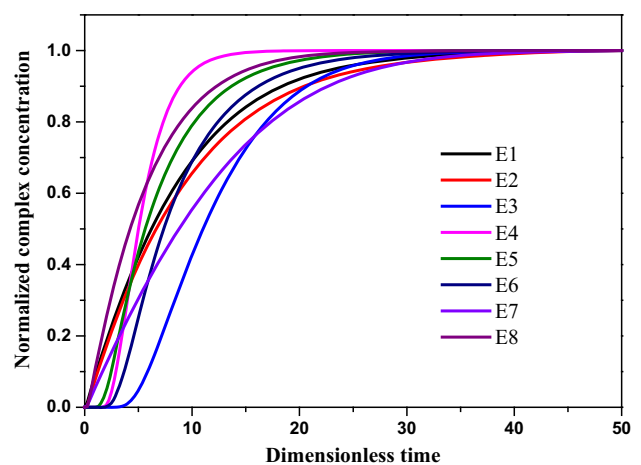


Fig. 5 Average normalized complex concentration for all experiment number

Table 5 Taguchi's L8(2⁵) orthogonal array and numerical results

Experiment number	Response time: T_R	S/N ratio (dB)
E1	23.5	- 27.42
E2	7.93	- 17.99
E3	0.48	6.38
E4	0.21	13.56
E5	0.40	9.37
E6	0.34	7.96
E7	5.47	- 14.76
E8	3.09	- 9.80

3.2. Analysis of means

The means is calculated with the following equation for all results:

$$\bar{T}_R = \frac{1}{8} \sum_{i=1}^8 T_{Ri} = 5.18 \tag{6}$$

3.3. Calculate average effect

The peak-to-peak average value of time response of factor A at level 1 is obtained with

$$\bar{T}_{RA_1}(T_R) = \frac{1}{4}(T_R(1) + T_R(2) + T_R(3) + T_R(4)) \tag{7}$$

where the factor is set to level 1 only in experiments 1–4. In a similar way, for all levels of factors, the peak-to-peak average value of response time can be calculated. Table 6 shows the results of peak-to-peak average values of response time for all levels of all factors. Figure 6 illustrates the main factor effects on response time. It is seen that the factor-level combination (A₂, B₂, C₂, D₂, E₂) contributes to minimization of response time.

3.4. Analysis of variance

To achieve a minimum response time of microfluidic biosensor, the influence of process parameters in terms of signal-to-noise ratio (SNR) is determined based on lower the better criteria since we want to minimize the detection

Table 6 Average peak-to-peak value of response time for all levels of all factors

Level	Re	Da	Σ	K_D	Sc
1	8.03	8.04	10	7.45	6.87
2	2.33	2.31	0.36	2.91	3.49
Max–min	5.07	5.73	9.64	1.54	3.38
Rank	3	2	1	5	4

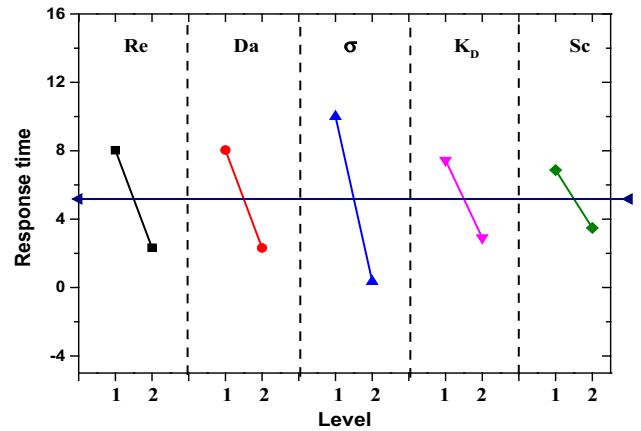


Fig. 6 Main factor effects on response time

time of the biosensor. The SNR for smaller the better is given by the following equation [46, 47]:

$$S/N = -10 \log_{10} \left(\frac{1}{n} \sum_{i=1}^n Y_i^2 \right) \tag{8}$$

The results are shown in main effect plot (Fig. 5) and ANOVA table (Table 7; Fig. 7).

In the response time of the microfluidic biosensor, the percentage of each key factor can be determined by analysis of variance (ANOVA). Table 7 gives the results of the ANOVA with respect to the key factors. The equations used in this analysis are as follows (Eqs. 9–13):

- The average of all response times \bar{T}_R is:

$$\bar{T}_R = \frac{1}{8} \sum_{i=1}^8 T_{Ri} \tag{9}$$

- The total sum of squares SS_{Total} is:

Table 7 Analysis of variance (ANOVA) for response time T_R

Symbol	Optimization parameter	DF	SS	MSS	F	Contribution %
Re	Reynolds number	1	65.094	65.094	2.17	14.77
Da	Damköhler number	1	65.666	65.666	2.19	14.9
σ	Relative adsorption capacity	1	185.859	185.859	6.19	42.17
K_D	Equilibrium constant	1	41.223	41.223	1.37	9.35
Sc	Schmidt number	1	22.849	22.849	0.76	5.19
Error		2	60.011	30.005		13.62
Total		7	440.702			

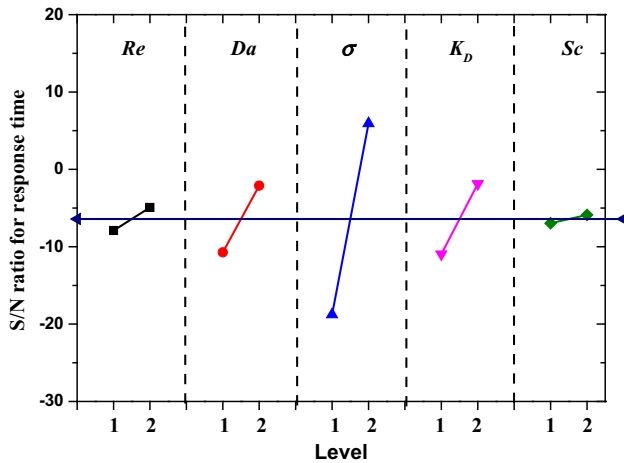


Fig. 7 Main effect plot of signal-to-noise ratio for response time

$$SS_{\text{Total}} = \sum_{i=1}^8 (T_{Ri} - \bar{T}_R)^2 \quad (10)$$

- The sum of squares for Reynolds number (Re), Damköhler number (Da), relative adsorption capacity (σ), equilibrium dissociation constant (K_D), and Schmidt number (Sc) are, respectively:

$$SS_i = 2 \sum_{i=1}^2 (T_{R_{xi}} - \bar{T}_R)^2 \quad (11)$$

where $T_{R_{xi}}$ is the i th average response time of the corresponding parameter x (Re , Da , σ , K_D and Sc) in the Taguchi design.

- the mean squares (MS) for each parameter i are expressed with:

$$MS_i = \frac{SS_i}{DF_i} \quad (12)$$

where DF is the degree of freedom (1 = number of level-1).

- The contribution percentages for each parameter i are:

$$\% \text{Contribution}_i = \frac{SS_i}{SS_{\text{Total}}} \quad (13)$$

It is clear from table (Table 7) that the relative adsorption capacity (σ) has the highest contribution (42.17%), and the Schmidt number (Sc) has the lowest contribution (5.19%) to reduce the response time among the five selected key parameters. Further, the contribution of the Reynolds number (Re), Damköhler number (Da) and equilibrium constant (K_D) to the minimization of response time is 14.77%, 14.90% and 9.35%, respectively. According to the principles presented by Taguchi, the outcomes are valid and trustworthy if the estimated error

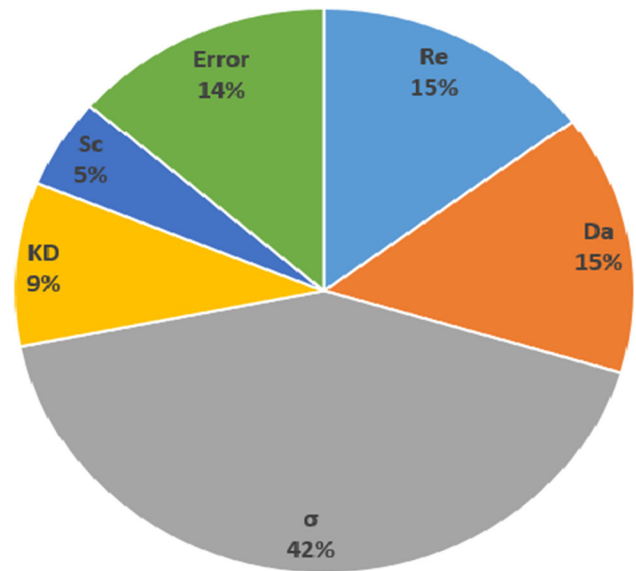


Fig. 8 Contribution of key parameters (Re , Da , σ , K_D , Sc) on the response time

from ANOVA is lower than 15% [48, 49]. Relevant results in Table 7 and Fig. 8 prove that error is 13.62%, and therefore, the results of response time are valid and trustworthy.

4. Conclusions

This study focuses on the optimization of some key parameters of a microfluidic biosensor for SARS-CoV-2 immunoassay using the Taguchi approach. Detection is based on the efficiency of the kinetics of the SARS-Cov-2 binding reaction. A first-order adsorption model is proposed to govern the binding reaction between ligands and analytes on the reaction surface to create analyte–ligand complexes. The analyte concentration is modeled by a stable distributed convection–diffusion equation in which the advection rate is assumed to satisfy the Navier–Stokes equation. Multiple numerical tests with critical parameters like Reynolds number (Re), Damköhler number (Da), relative adsorption capacity (σ), equilibrium dissociation constant (K_D) and Schmidt number (Sc) at two levels are performed. The novelty of this study is the use of Taguchi’s method in the optimization analysis through an $L8(2^5)$ orthogonal array of five key parameters. ANOVA methods are also used to obtain the meaning of these key parameters.

The optimal combination of these parameters is obtained for $Re = 10^{-2}$, $Da = 1000$, $\sigma = 0.2$, $K_D = 5$ and $Sc = 10^4$, giving the minimum dimensionless response time (0.15).

References

- [1] I Santiago *ChemBioChem* **21** 2880 (2020)
- [2] N ben Khedher, L Kolsi and H Alsaif *Alexandria Engineering Journal* **60** 3965 (2021)
- [3] L Dai Tran, B H Nguyen, N Van Hieu, H V Tran, H Le Nguyen and P X Nguyen *Materials Science and Engineering:C* **31** 477 (2011)
- [4] S Haerberle and R Zengerle *Lab on a Chip* **7** 1094 (2007).
- [5] J R Choi *Frontiers in chemistry* **8** 517 (2020)
- [6] D H Ko, A Hosseini, H Karaosmanoglu, K Taredun, L Jones and A Partridge *Sensors and Actuators B:Chemical* **351** 130918 (2022)
- [7] A Parihar, P Ranjan, S K Sanghi, A K Srivastava and R Khan *ACS applied bio materials* **3** 7326 (2020)
- [8] V Kanda, J K Kariuki, D J Harrison and M T McDermott *Analytical Chemistry* **76** 7257 (2004)
- [9] K H Lee, Y D Su, S J Chen, F G Tseng and G B Lee *Biosensors and Bioelectronics* **23** 466 (2007)
- [10] F Pascal-Delannoy, B Sorli and A Boyer *Sensors and Actuators A: Physical* **84** 285 (2000)
- [11] X C Zhou, L Q Huang and S F Y Li *Biosensors and Bioelectronics* **16** 85 (2001)
- [12] K A Eberhardt et al *Microorganisms* **9** 733 (2021).
- [13] E Mohit, Z Rostami and H Vahidi *Expert review of clinical immunology* **17** 573 (2021)
- [14] K R Huang and J S Chang *Heat and Mass Transfer* **49** 1647 (2013).
- [15] F Echouchene, T Al-shahrani and H. Belmabrouk *Applied Sciences* **11** 4566 (2021)
- [16] F Echouchene, T Al-Shahrani and H. Belmabrouk *Sensors* **21** 3502 (2021)
- [17] S Kaziz, I Ben Mariem, F Echouchene, M Belkhiria and H Belmabrouk *The European Physical Journal Plus* **137** 1 (2022)
- [18] S Kaziz, I Ben Mariem, F Echouchene, M H Gazzah and H Belmabrouk *Indian Journal of Physics* **96** 4091 (2022)
- [19] S Kaziz, Y Saad, M Bouzid, M Selmi and H Belmabrouk *Microfluidics and Nanofluidics* **25** 1 (2021)
- [20] S Kaziz, Y Saad, M H Gazzah and H Belmabrouk *The European Physical Journal Plus* **137** 1 (2022)
- [21] M Selmi, F Echouchene and H Belmabrouk *Sensor Letters* **14** 26 (2016)
- [22] M Selmi, F Echouchene, M H Gazzah and H Belmabrouk *IEEE Sensors Journal* **15** 7321 (2015)
- [23] M Selmi, R Khemiri, F Echouchene and H Belmabrouk *Journal of Manufacturing Science and Engineering* **138** (2016)
- [24] M Selmi, R Khemiri, F Echouchene and H Belmabrouk *Applied Thermal Engineering* **105** 77 (2016)
- [25] O Hofmann, G Voirin, P Niedermann and A Manz *Analytical chemistry* **74** 5243 (2002)
- [26] M Selmi and H Belmabrouk *Micromachines* **11** 342 (2020).
- [27] Y Huang, C Yang, X F Xu, W Xu and S W Liu *Acta Pharmaceutologica Sinica* **41** 1141 (2020)
- [28] V M Corman et al *Eurosurveillance* **25** 2000045 (2020).
- [29] C T Pachucki, M A Khurshid and J Nawrocki *Journal of clinical microbiology* **42** 2796 (2004)
- [30] M Selmi, M H Gazzah and H Belmabrouk *Scientific Reports* **7** 1 (2017)
- [31] F Shahbazi, M Jabbari, M N Esfahani and A Keshmiri *Biosensors and Bioelectronics* **171** 112716 (2021)
- [32] H Hajji, L Kolsi, K Ghachem, C Maatki and M N Borjini *Alexandria Engineering Journal* **59** 1649 (2020)
- [33] H Hajji, L Kolsi, W Hassen, A A Al-Rashed, M N Borjini and M A Aichouni *Physica E: Low-dimensional Systems and Nanostructures* **104** 177 (2018)
- [34] M A Sayed, O M Dawood, A H Elsayed and W R Daoush *Advances in materials Research* **6** 079 (2017).
- [35] S Kaziz, I Ben Romdhane, F Echouchene and M H Gazzah *The European Physical Journal Plus* **138** 96 (2023)
- [36] C H Wu and W S Chen *Sensors and Actuators A: Physical* **125** 367 (2006).
- [37] N Daneshvar, A Khataee, M Rasoulifard and M Pourhassan *Journal of Hazardous Materials* **143** 214 (2007)
- [38] B J du Plessis and G De Villiers *Resources, Conservation and Recycling* **50** 202 (2007)
- [39] J Y Houg, J H Liao, J Y Wu, S C Shen and H F Hsu *Process Biochemistry* **42** 1 (2007)
- [40] R Romero-Villafranca, L Zúnica and R Romero-Zúnica *Journal of Statistical planning and inference* **137** 1488 (2007)
- [41] J A Thompson and H H Bau *Journal of Chromatography B* **878** 228 (2010)
- [42] J Berthier and P Silberzan *Microfluidics for biotechnology* (Artech House) (2010)
- [43] M Zimmermann, E Delamarche, M Wolf and P Hunziker *Biomedical microdevices* **7** 99 (2005)
- [44] C Qi et al *Biomedical microdevices* **8** 247 (2006).
- [45] Z Chen *Computers & Mathematics with Applications* **25** 81 (1993)
- [46] A Bagchi, S Saravanan, G S Kumar, G Murugan and K Raghukandan *Optik* **146** 80 (2017)
- [47] J H Sun, Y C Fang and B R. Hsueh *Optik* **123** 1768 (2012)
- [48] P Rana and G Gupta *International Communications in Heat and Mass Transfer* **130** 105822 (2022)
- [49] R K Roy, *Design of experiments using the Taguchi approach: 16 steps to product and process improvement* (John Wiley & Sons) (2001)

Publisher's Note Springer Nature remains neutral with regard to jurisdictional claims in published maps and institutional affiliations.

Springer Nature or its licensor (e.g. a society or other partner) holds exclusive rights to this article under a publishing agreement with the author(s) or other rightsholder(s); author self-archiving of the accepted manuscript version of this article is solely governed by the terms of such publishing agreement and applicable law.